Iraqi Journal of Science, 2020, Vol. 61, No. 7, pp: 1733-1744
DOI: 10.24996/ijs.2020.61.7.22

ISSN: 0067-2904

Numerical Study of Radiative Magnetohydrodynamics Viscous Nanofluid Due to Convective Stretching Sheet with the Chemical Reaction Effect

G. Narender[1]*, K. Govardhan[2], G. Sreedhar Sarma[1]
[1]Department of Humanities and Sciences (Mathematics), CVR College of Engineering, Hyderabad, Telangana State, India
[2]Depaertment of Mathematics, GITAM University, Hyderabad, Telangana State, India

Received: 27/9/2019 Accepted: 30/11/2019

ABSTRACT

A numerical investigation was performed for the radiative magnetohydrodynamic (MHD) viscous nanofluid due to convective stretching sheet. Heat and mass transfer were investigated in terms of viscous dissipations, thermal radiation and chemical reaction. The governing Partial Differential Equations (PDEs) were transformed into an arrangement of non-linear Ordinary Differential Equations (ODEs) by using the similarity transformation. The resulting system of ODEs is solved numerically by using shooting method along with Adams-Moulton Method of order four with the help of the computational software FORTAN. Furthermore, we compared our results with the existing results for especial cases. which are in an excellent agreement. The numerical solution obtained the velocity, temperature and concentration profiles. The figures showed differences among the parameters. Moreover, the numerical values of Nusselt and Sherwood numbers were presented and analyzed through tables.

Keywords: Magnetic Effect; Nanofluid; Convective Boundary Condition; Viscous Dissipation; Chemical Reaction.

1. INTRODUCTION

The transfer of heat by the movement of fluids from one place to another is called convective heat transfer, which is a combination of heat diffusion and bulk fluid flow, that are called conduction and advection, respectively. In engineering problems, convective heat transfer has wide applications. A large number of investigations on nanofluids (i.e. the mixture of fluid and nanoparticles) showed that this approach can improve thermal conductivity in fluids. Nanofluid is a fluid containing nanometer-sized particles called nanoparticles, which are made of metals, oxides, carbides, etc. Nanofluids have properties that make them potentially useful in many heat transfer applications. They exhibit enhanced thermal conductivity and convective heat transfer coefficient. Choi [1] studied the enhancement of thermal conductivity of fluids with nanoparticles. Eastman *et al*. [2] reviewed the detailed work performed on convective transport in nanofluids. The different theories of heat transfer in nanofluids were discussed by Boungiorno [3]. Kuznetsov and Nield [4] studied the convective nanofluid in a vertical plate, and later they extended their work for porous medium as well [5].

The impact of thermal rays is essential in space technology and high temperature processes. At the point when the temperature variation is very high, the linear thermal radiation causes a noticeable error. To overcome such errors, nonlinear thermal radiation is taken into account. The impact of the chemical reaction and thermal radiation on the flow over a stretching surface with an outer heat source was explained by Krishna *et al*. [6]. Researchers conducted a series of research work to highlight the importance of thermal radiation [7-9].

*Email: gnriimc@gmail.com

The chemical reaction can further be classified by considering the heterogeneous and homogenous processes. In the case of a strong compound system, the reaction is heterogeneous. In most of the cases of chemical reaction processes, the concentration rate depends upon the species itself, as discussed by Magyari *et al*. [10]. Devi and Kandasmy [11] analyzed the impact of the homogenous chemical reaction with heat and mass transfer laminar flow along with semi-infinite horizontal plate. Chamkha and Rashad [12] described the impact of the chemical reaction on MHD flow in the presence of heat generation or absorption of uniform vertical permeable surface. In addition, many significant features of the MHD flow past a stretching sheet were presented and elaborated in the literature [13-15].

In this article, we present a review study of Gbadeyan *et al*. [16] and then extend the flow analysis with variable thermophysical properties. Also, we present a comparison of the obtained numerical results with those from a previously published study [16]. The results showed that both approaches are in excellent agreement.

2. MATHEMATICAL FORMULATION

Let us consider the numerical investigation of MHD boundary layer flow of an incompressible nanofluid. The flow is two-dimensional that passes a stretching surface with a porous medium. The plate is stretched with a velocity of $u_w = ax$, where a is a constant along $x-$direction. In addition, the fluid is flowing in the presence of a magnetic field which is supposed to be applied along the $y-$direction. The temperature at surface is T_w, whereas C_w represents the nanoparticle concentration at surface. The uniform temperature and the nanofluid volume fraction far from the surface of the sheet are T_∞ and C_∞ respectively, as y tends to ∞.

The following system of equations is incorporated for the mathematical model [16]:

$$\frac{\partial u}{\partial x}+\frac{\partial v}{\partial y}=0, \tag{1}$$

$$u\frac{\partial u}{\partial x}+v\frac{\partial u}{\partial y}=-\frac{1}{\rho}\frac{\partial p}{\partial x}+\nu\left(\frac{\partial^2 u}{\partial x^2}+\frac{\partial^2 u}{\partial y^2}\right)+\frac{\sigma B_0^2}{\rho_f}u,, \tag{2}$$

$$u\frac{\partial \mathrm{v}}{\partial x}+\mathrm{v}\frac{\partial \mathrm{v}}{\partial y}=-\frac{1}{\rho}\frac{\partial p}{\partial y}+\nu\left(\frac{\partial^2 \mathrm{v}}{\partial x^2}+\frac{\partial^2 \mathrm{v}}{\partial y^2}\right)+\frac{\sigma B_0^2}{\rho_f}v, \tag{3}$$

$$u\frac{\partial T}{\partial x}+\mathrm{v}\frac{\partial T}{\partial y}=\frac{\mu}{C_p}\left(\frac{\partial u}{\partial y}\right)^2+\alpha\left(\frac{\partial^2 T}{\partial x^2}+\frac{\partial^2 T}{\partial y^2}\right)+\tau\left[D_B\frac{\partial C}{\partial y}\frac{\partial T}{\partial y}+\frac{D_T}{T_\infty}\left(\frac{\partial T}{\partial y}\right)^2\right]-\frac{\alpha}{\rho_f}\left(\frac{\partial q_r}{\partial y}\right) \tag{4}$$

$$u\frac{\partial C}{\partial x}+\mathrm{v}\frac{\partial C}{\partial y}=D_B\left(\frac{\partial^2 C}{\partial x^2}+\frac{\partial^2 C}{\partial y^2}\right)+\frac{D_T}{T_\infty}\frac{\partial^2 T}{\partial y^2}-K_0\left(C-C_\infty\right) \tag{5}$$

Where u and v are the components of velocity in the x and y directions, respectively, (see Nomenclature table).

The associated boundary conditions for the above system are

$$\left.\begin{aligned} &u=u_w\left(x\right)=ax, v=0, -k_f\frac{\partial T}{\partial y}=h\left(T_f-T\right), -C=C_w \quad at \quad y=0\\ &u=0,\ v=0,\ T\to T_\infty,\ C\to C_\infty \quad as \quad y\to\infty \end{aligned}\right\} \tag{6}$$

The radiative heat flux q_r is given as [13]

$$q_r=\frac{-4\sigma^*}{3k^*}\frac{\partial T^4}{\partial y} \tag{7}$$

This can be expanded with the help of Taylor series along with T_∞ [15], as follows:

$$T^4=T_\infty^4+\frac{4T_\infty^3}{1!}\left(T-T_\infty\right)+\frac{12T_\infty^2}{2!}\left(T-T_\infty\right)^2+\frac{24T_\infty^3}{3!}\left(T-T_\infty\right)^3+..... \tag{8}$$

By rewriting equation (8) and ignoring higher order terms, we have

$$T^4 = T_\infty^4 + \frac{4T_\infty^3}{1!}\left(T - T_\infty\right) \Rightarrow T^4 = 4T_\infty^3 T - 3T_\infty^4 \tag{9}$$

By substituting (9) into (7), we get

$$\frac{\partial q_r}{\partial y} = -\frac{16\sigma^* T_\infty^3}{3k^*}\frac{\partial^2 T}{\partial y^2}, \tag{10}$$

The stream function $\psi = \psi(x,y)$ is identically satisfying continuity equation. Mathematically,

$$u = \frac{\partial \psi}{\partial y}, v = -\frac{\partial \psi}{\partial x} \tag{11}$$

The following process was implemented to convert the PDEs to ODEs [16]:

$$\eta = y\sqrt{\frac{a}{\nu}},\ \psi(x,y) = \sqrt{a\nu}\,x f(\eta),\ \theta(\eta) = \frac{T - T_\infty}{T_f - T_\infty},\ \ \beta(\eta) = \frac{C - C_\infty}{C_w - C_\infty} \tag{12}$$

The final dimensionless form of the governing model is [16]:

$$f'''(\eta) + f(\eta) f''(\eta) - \left(f'(\eta)\right)^2 + Mf'(\eta) = 0, \tag{13}$$

$$\frac{\left(1+\frac{4}{3}R\right)}{\Pr}\theta''(\eta) + f(\eta)\theta'(\eta) + Nb\theta'(\eta)\beta'(\eta) + Nt\left(\theta'(\eta)\right)^2 + Ec\left(f''(\eta)\right)^2 = 0, \tag{14}$$

$$\beta''(\eta) + Le\, f(\eta)\beta'(\eta) + \frac{Nt}{Nb}\theta''(\eta) - Le\ \chi\beta(\eta) = 0. \tag{15}$$

The BCs have the form:

$$\left.\begin{aligned} &f(\eta) = 0,\quad f'(\eta) = 1,\ \ \theta'(\eta) = -Bi\left[1 - \theta(0)\right],\ \ \beta(0) = 1,\quad at\quad \eta = 0,\\ &f'(\eta) \to A,\quad \theta(\eta) \to 0,\quad \beta(\eta) \to 0\quad as\quad \eta \to \infty. \end{aligned}\right\} \tag{16}$$

The equations for the dimensional form of skin-friction coefficient, Nusselt number, and Sherwood number, respectively, are as follows:

$$C_f\,\mathrm{Re}_x^{1/2} = -f''(0)\frac{Nu}{\sqrt{\mathrm{Re}_x}} = -\theta'(0),\ \frac{Sh}{\sqrt{\mathrm{Re}_x}} = -\beta'(0) \tag{17}$$

3. NUMERICAL ANALYSIS

The set of non-linear coupled differential equations (13) - (15) with the conditions (16) is solved numerically. Firstly, it is noticed that the heurist infinity for the independent variable is selected as η_{max}.

Equation (13) is solved with $f''(0) = \alpha$, using the initial conditions

$$f(0) = 0,\ f'(0) = 1,\ f''(0) = \alpha \tag{18}$$

α is iteratively found using Newton's method, $F'(\eta_{max}) = \frac{\partial}{\partial\alpha}\left(f'(\eta_{max})\right)$ which is obtained by solving,

$$F''' = 2f'F' - fF'' - f''F' + Mf', \tag{19}$$

with $F(0) = 0, F'(0) = 0$ and $F''(0) = 1$. (20)

After finding $f(\eta)$ we solved equations (14) and ((15) with the initial condition (16).

Thereby, the following notations were considered.

$$\left.\begin{aligned}&\theta = y_1, \theta^{'} = y_2, \beta = y_3, \beta^{'} = y_4, \frac{\partial \theta}{\partial l} = y_5, \frac{\partial \theta^{'}}{\partial l} = y_6, \frac{\partial \beta}{\partial l} = y_7\\ &\frac{\partial \beta^{'}}{\partial l} = y_8, \frac{\partial \theta}{\partial m} = y_9, \frac{\partial \theta^{'}}{\partial m} = y_{10}, \frac{\partial \beta}{\partial m} = y_{11}, \frac{\partial \beta^{'}}{\partial m} = y_{12}.\end{aligned}\right\}. \quad (21)$$

By incorporating the above notations, a system of first order ODEs is achieved, that is stated below.

$$\begin{bmatrix} y_1^{'} \\ y_2^{'} \\ y_3^{'} \\ y_4^{'} \end{bmatrix} = \begin{bmatrix} y_2 \\ \dfrac{-Pr\left(FF(I)y_2 + Nby_2y_4 + Nty_2^2 + Ec\,F^{''}\left(\eta_{max}\right)\right)}{\left(1+\frac{4}{3}R\right)} \\ y_4 \\ -LeFF(I)y_4 - \dfrac{Nt}{Nb}y_2^{'} + Le\gamma y_6 \end{bmatrix} \quad (22)$$

The associated boundary conditions can be written as

$$\begin{bmatrix} y_1(0) \\ y_2(0) \\ y_3(0) \\ y_3(0) \end{bmatrix} = \begin{bmatrix} p_1 \\ Bi(p-1) \\ 1 \\ p_2 \end{bmatrix} \quad (23)$$

Here $p_1 = \theta(0)$ and $p_2 = \beta^{'}(0)$. p_1 and p_2 are to be found and satisfying the end conditions $y_1 \to 0, y_3 \to 0$ as $\eta \to 0$.

Adams Moultan fourth order method (with the corresponding predictor) is used to solve the initial value problem. Assumed values of p_1 and p_2 are corrected using Newton's method.

This system is solved with the three different sets of initial conditions of $y_i(0) = 0$ for all $i = 1,2,3,4$.

Newton's method is expressed as

$$\begin{bmatrix} p_1 \\ p_2 \end{bmatrix}^{new} = \begin{bmatrix} p_1 \\ p_2 \end{bmatrix}^{old} - \begin{bmatrix} \dfrac{\partial y_1}{\partial p_1} & \dfrac{\partial y_1}{\partial p_2} \\ \dfrac{\partial y_2}{\partial p_1} & \dfrac{\partial y_2}{\partial p_2} \end{bmatrix}^{-1}_{\eta_{max}} \begin{bmatrix} y_1 \\ y_2 \end{bmatrix} \quad (24)$$

Derivatives of $\theta(\infty, p_1, p_2)$ and $\beta(\infty, p_1, p_2)$ with respect to any parameter $p(\,p_1 \ or \ p_2\,)$ are found by solving the equation obtained by the differentiating system (21).

$Y_i = \dfrac{\partial y_i}{\partial p}$ for all $i = 1,2,3,4$. Such that,

$$Y_1^{'} = Y(2),$$

$$Y_2^{'} = \frac{-Pr}{\left(1+\frac{4}{3}R\right)}\left[FF(I)Y(2) + Nb\left(y(2))Y(4) + y(4)Y(2)\right)\right] + 2Nty(2))Y(2),$$

$$Y_3^{'} = Y(4),$$

$$Y_4^{'} = -LeFF(I)y(4) - \frac{Nt}{Nb}Y_2^{'} + Le\ \gamma\, y(3).$$

It should be noticed that the choice of initial guess of p_1, p_2 is very crucial. Once we obtain a solution for a set of physical parameters, a single parameter is changed slightly to achieve convergence of Newton's method. Moreover, $\eta_{max} = 8$ is more than enough for the end condition. The convergence criteria are selected to be successive values of agreement up to 3 significant digits.

4. RESULTS AND DISCUSSION

Gbadeyan [16] used a six order Runge-Kutta method for the numerical solution of the discussed model. In the present survey, the shooting technique along with Adams-Moulton Method of fourth order were opted for reproducing the solution of [16]. In Tables- 1 and 2, comparisons of Nusselt number and Sherwood number for different values of Nt and Nt are displayed. We compared the results with those of the published work of Gbadeyan [16], with a good agreement of numerical results being achieved.

As a test of the accuracy of our numerical computations in Table- 3, the values of $-\theta'(0)$ and $-\beta'(0)$ were compared with Gbadeyan [13], with the results showing an agreement with each other. In Table- 4, we discuss the effects of Prandtl number, Biot number and Lewis number on reduced Nusselt Sherwood numbers and the surface temperature of the stretching sheet.

Table 1-Comparison of the computed values of Nusselt number $-\theta'(0)$ when $Pr = Le = 10, Bi = 0.1, M_x = Ra = Ec = \chi = 0.$

Nt	$Nb = 0.1$		$Nb = 0.2$		$Nb = 0.3$		$Nb = 0.4$		$Nb = 0.5$	
	Gbadeyan, [16]	Present results	Gbadeyan, [16]	Present results	Gbadeyan, [16]	Present results	Gbadeyan, [16]	Present results	Gbadeyan, [16]	Present results
0.1	0.0929	0.0929073	0.0873	0.0873322	0.0769	0.0768783	0.0597	0.0596645	0.0383	0.0383333
0.2	0.0927	0.0927325	0.0868	0.0867621	0.0751	0.0750821	0.0553	0.0553488	0.0325	0.0324988
0.3	0.0925	0.0925451	0.0861	0.0861186	0.0729	0.0729169	0.0503	0.0502681	0.0269	0.0268967
0.4	0.0923	0.0923436	0.0854	0.0853850	0.0703	0.0702650	0.0445	0.0445494	0.0220	0.0219939
0.5	0.0921	0.0921259	0.0845	0.0845383	0.0700	0.0669740	0.0386	0.0385990	0.0180	0.0180108

Table 2-Comparison of the computed values of $-\beta'(0)$ when $Pr = Le = 10, Bi = 0.1, M_x = Ra = Ec = \chi = 0.$

Nt	$Nb = 0.1$		$Nb = 0.2$		$Nb = 0.3$		$Nb = 0.4$		$Nb = 0.5$	
	Gbadeyan, [16]	Present results	Gbadeyan, [16]	Present results	Gbadeyan, [16]	Present results	Gbadeyan, [16]]	Present results	Gbadeyan, [16]	Present results
0.1	2.2774	2.2773990	2.3109	2.3109240	2.3299	2.3299260	2.3458	2.3458080	2.3560	2.3560170
0.2	2.2490	2.2489400	2.3168	2.3167950	2.3569	2.3569050	2.3903	2.3902290	2.4071	2.4070820
0.3	2.2228	2.2227930	2.3261	2.3260420	2.3900	2.3899490	2.4411	2.4411120	2.4576	2.4576010
0.4	2.1992	2.1991730	2.3392	2.3392140	2.4303	2.4302830	2.4967	2.4966420	2.5039	2.5038240
0.5	2.1783	2.1783270	2.3570	2.3570160	2.4792	2.4792030	2.5529	2.5528370	2.5435	2.5434770

Table 3-Comparison of the computed values of reduced Nusselt number $-\theta'(0)$, reduced Sherwood number $-\beta'(0)$ and surface temperature $\theta(0)$ with $Nt = Nb = 0.5, M_x = Ra = Ec = \chi = 0$.

Pr	Bi	Le	$-\theta'(0)$		$-\beta'(0)$		$-\theta(0)$	
			Gbadeyan, [16]	Present results	Gbadeyan, [16]	Present results	Gbadeyan, [16]	Present results
1	0.1	5	0.0789	0.0790023	1.5477	1.5480090	0.2107	0.2099772
2	0.1	5	0.0806	0.0806179	1.5554	1.5554070	0.1938	0.1938211
5	0.1	5	0.0735	0.0734504	1.5983	1.5982920	0.2655	0.2654958
10	0.1	5	0.0387	0.0386823	1.7293	1.7292380	0.6132	0.6131769
5	1.0	5	0.1476	0.1475660	1.6914	1.6913280	0.8524	0.8524340
5	10.0	5	0.1550	0.1550132	1.7122	1.7121770	0.9845	0.9844987
5	100	5	0.1557	0.1556586	1.7144	1.7143210	0.9984	0.9984465
5	∞	5	0.1557	0.1556864	1.7146	1.7144390	1.0000	0.9992254
5	0.1	10	0.0647	0.0646868	2.3920	2.3919500	0.3531	0.3531319
5	0.1	15	0.0600	0.0599905	2.9899	2.9899190	0.4001	0.4000952
5	0.1	20	0.0570	0.0570399	3.4881	3.4881270	0.4296	04296013

Table 4- Computations showing the reduced Nusselt number $-\theta'(0)$, reduced Sherwood number $-\beta'(0)$ and surface temperature $\theta(0)$ with $Nt = Nb = 0.5$

Pr	Bi	Le	M_x	Ec	χ	Ra	Nur	Shr	$\theta(0)$
1	0.1	5	1	0.5	0.5	1	0.0676718	2.1657110	0.3232823
2	0.1	5	1	0.5	0.5	1	0.0745104	2.1689580	0 .2548957
5	0.1	5	1	0.5	0.5	1	0.0773816	2.1871280	0 .2261845
10	0.1	5	1	0.5	0.5	1	0.0703142	2.2380760	0.2968582
5	1.0	5	1	0.5	0.5	1	0.2094531	2.2598310	0 .7905469
5	10.0	5	1	0.5	0.5	1	0.2388047	2.2861200	0 .9761195
5	100	5	1	0.5	0.5	1	0.2418041	2.2891810	0 .9975820
5	∞	5	1	0.5	0.5	1	0.2420053	2.2893890	0.9990358
5	0.1	9	1	0.5	0.5	1	0.0759846	2.9943290	0 .2401544
5	0.1	13	1	0.5	0.5	1	0.0752678	3.6325080	0.2473217
5	0.1	15	1	0.5	0.5	1	0.0750203	3.9139790	0.2497970
5	0.1	5	1.2	0.5	0.5	1	0.0770031	2.1799850	0.2299689
5	0.1	5	1.4	0.5	0.5	1	0.0766346	2.1732870	0 .2336541
5	0.1	5	1	0.5	0.5	1.4	0.0775752	2.1804510	0.2242482
5	0.1	5	1	0.5	0.5	1.7	0.0774202	2.1772350	0.2257977
5	0.1	5	1	0.5	0.5	2.0	0.0771237	2.1749030	0.2287629
5	0.1	5	1	1.0	0.5	1	2.7199620	2.7199620	0.2334387
5	0.1	5	1	0.05	0.5	1	0.0658030	2.230043	0.3419701
5	0.1	5	1	0.5	0.5	1	-0.0901763	2.6716640	1.9017630
5	0.1	5	1	0.5	-0.5	1	-0.1082383	0.3185525	2.0823830
5	0.1	5	1	0.5	0.0	1	-0.0827194	1.7871850	1.8271940
5	0.1	5	1	0.5	0.5	1	-0.0878605	2.6753770	1.8786050

Figure-1 shows the impact of the magnetic parameter on temperature profile. The resistive force generated due to the interaction of the conducting fluid and the magnetic field reduces the temperature at all points with a transverse compression of profiles reducing the thermal boundary layer thickness due to transverse magnetic field.

The influence of the thermal radiation parameter on the profile of temperature distribution is displayed in Figure-2 By increasing R, temperature profile increases significantly. The figure indicates that the thermal radiation is responsible for the enhancement of the thermal boundary layer thickness.

The impact of the Prandtl number for the variation of temperature distribution is visualized in Figure-3. This figure provides the evidence that the fluid with increasing values of the Prandtl number represents a weak energy diffusion. Thus, higher values of the Prandtl number result in a strong reduction in temperature profile.

Figures-(4 and 5) explain the effects of the Biot number (Bi) on temperature and concentration distribution. Increasing the value of dimensionless parameter (Bi) increases temperature and concentration distribution. Physically, the Biot number is basically the ratio between resistance of the heat transfer in the body and resistance at body surface. This is because of the fact that the convective heat exchange along the surface will enhance the momentum boundary layer.

Figures 6 and 7 are presented to visualize the effects of the thermophoresis parameter and Brownian motion= on temperature and concentration profiles, respectively. In these figures, it is observed that temperature and concentration profiles show an increment in response to growing values of the dimensionless parameters (Nt and Nb). Physically, heated particles leave away from high temperature to low temperature so that the temperature of the fluid increases.

The results of the concentration vs. Lewis number are illustrated in Figure 8. Increasing Le corresponds to the increase in concentration. As a result, the concentration on the surface increases initially, but after a while, it starts to decrease at a short distance away from the surface.

Figure 9 shows the influence of Eckert number (Ec) on the dimensionless temperature profile. Eckert number is the ratio of the kinetic energy dissipated in the flow to the thermal energy conducted into or away from the fluid. As shown in the figure, temperature profile increases with the increase in the values of Ec.

In Figure-10, we can see the impact of reaction rate χ on concentration profile. When the chemical reaction parameter χ increases, the boundary layer thickness decreases. This is due to the fact that the chemical reaction in this system results in consumption of the chemical and results in decrease of concentration profile.

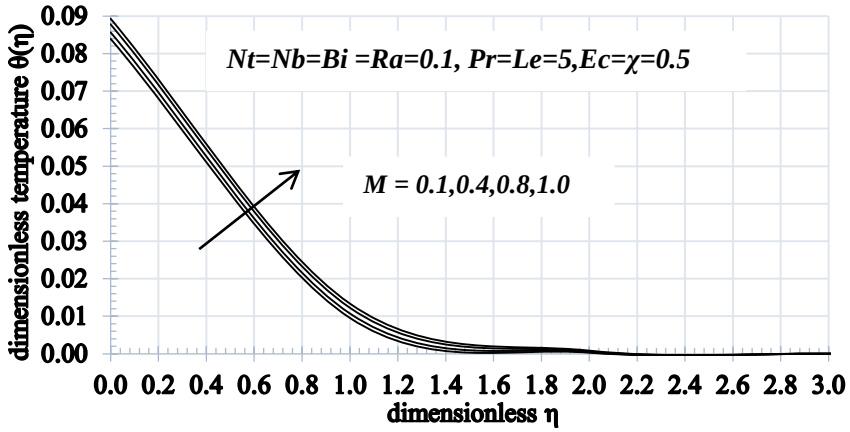

Figure 1-Impacts of M on the unitless energy $\theta(\eta)$.

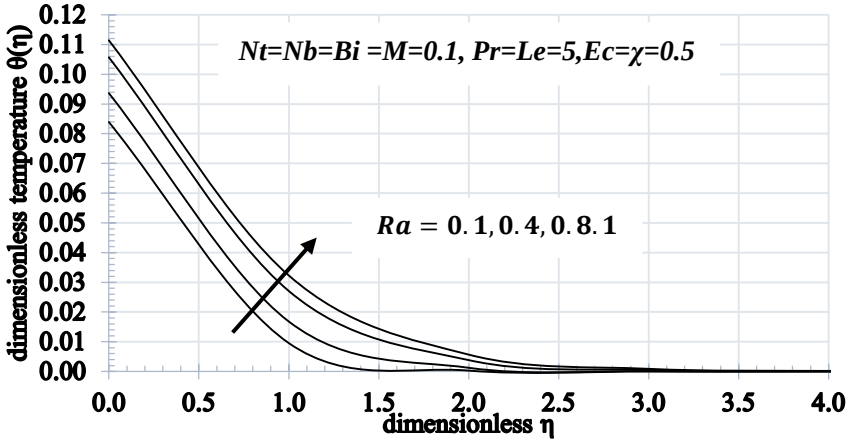

Figure 2-Impacts of Ra on the unitless energy $\theta(\eta)$

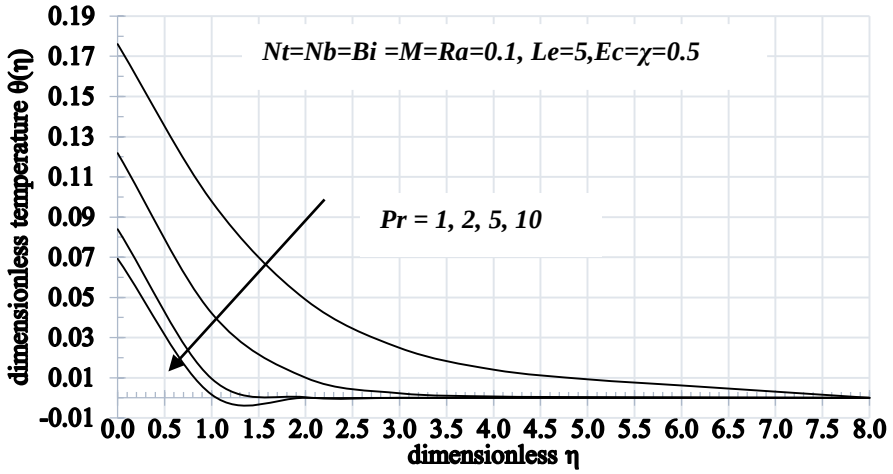

Figure 3-Impacts of Pr on the unitless energy $\theta(\eta)$.

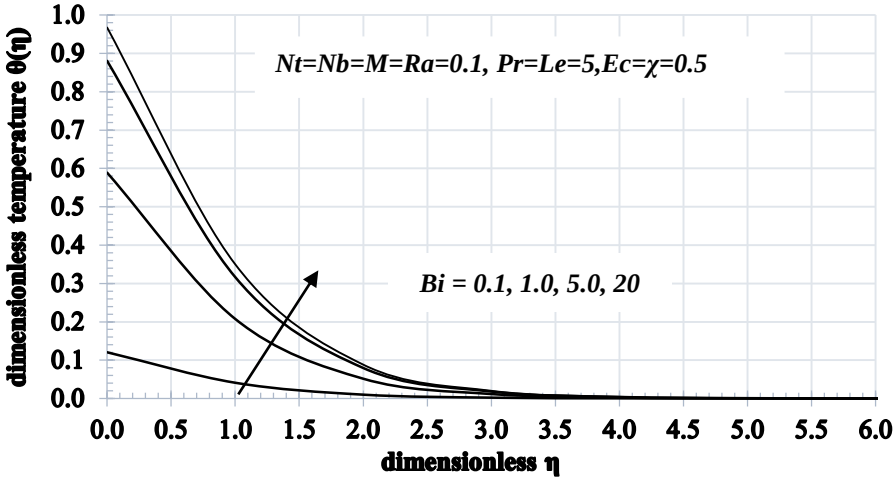

Figure 4- Impacts of Bi on the unitless energy $\theta(\eta)$.

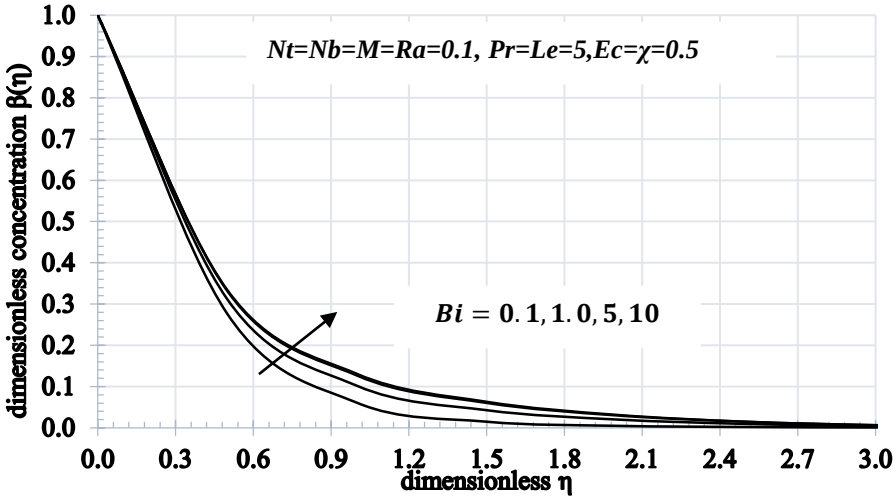

Figure 5-Impacts of Bi on the unitless concentration $\beta(\eta)$

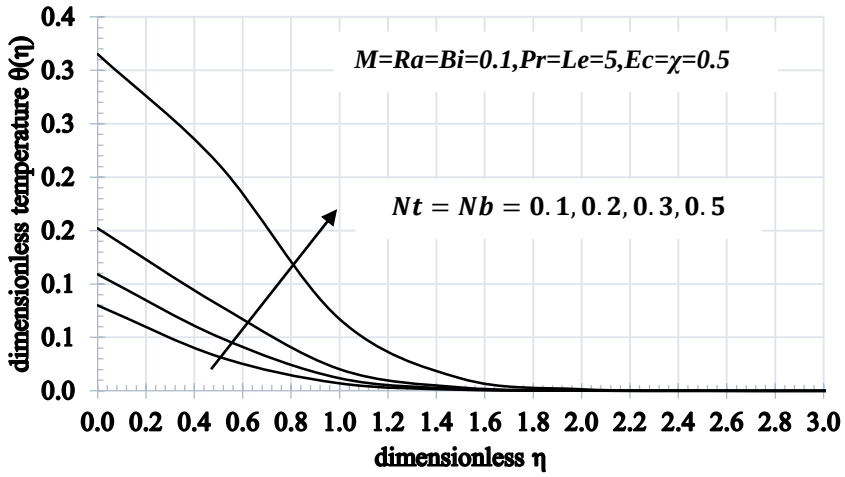

Figure 6-Impacts of Nt and Nb on the unitless energy $\theta(\eta)$

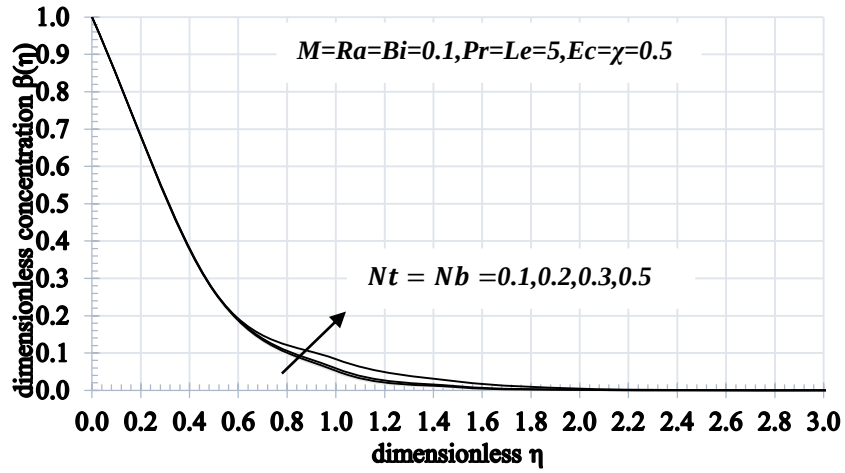

Figure 7-Impacts of Nt and Nb on the unitless concentration $\beta(\eta)$.

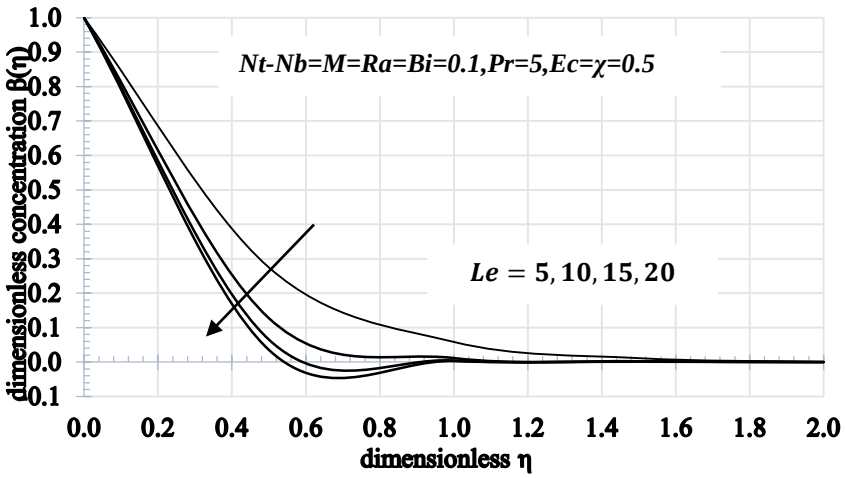

Figure 8-Impacts of Le on the unitless concentration $\beta(\eta)$.

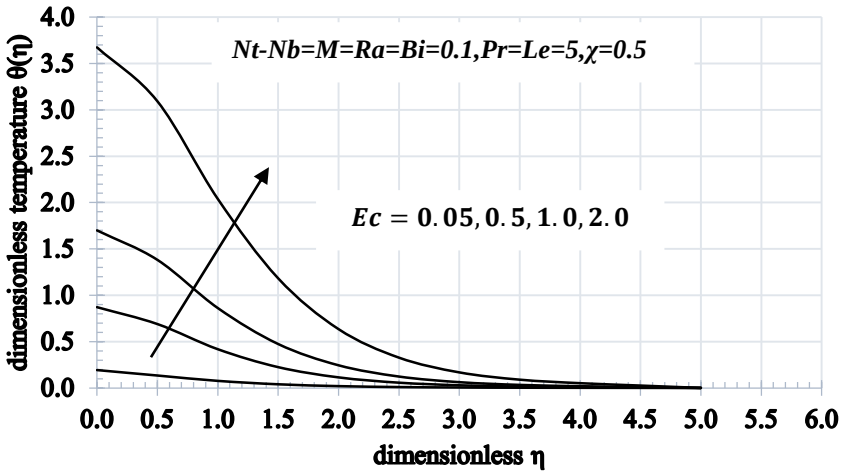

Figure 9-Impacts of Ec on the unitless energy $\theta(\eta)$.

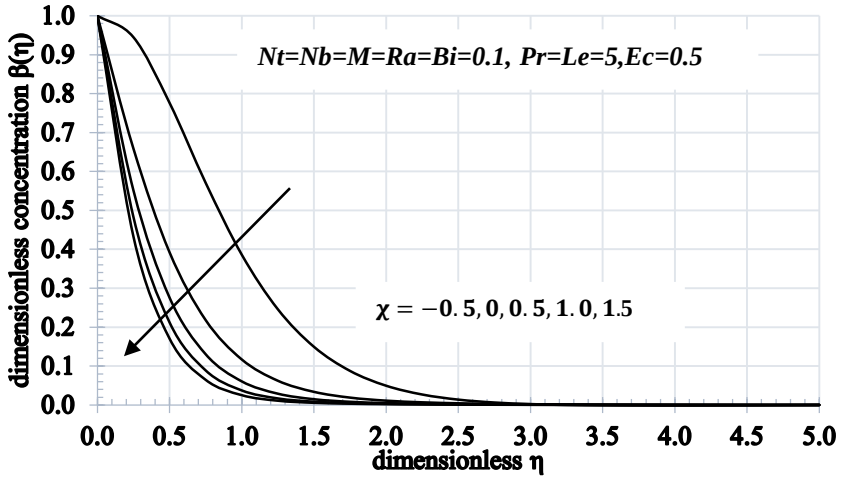

Figure 10-Effects of χ on concentration profiles $\beta(\eta)$.

5. CONCLUSION

After a thorough investigation, we have reached the following conclusions:

Higher values of magmatic parameter M and radiation parameter Ra enhance the temperature profile. Temperature profile increases due to the increase in the Ec. The concentration boundary layer thickness is becoming thinner with increasing Lewis number Le. Both temperature and concentration profiles are increased by increasing the value of Biot number Bi. The mass transfer decreases with increasing the chemical reaction parameter. The increase in Prandtl number Pr decreases the temperature.

ACKNOWLEDGMENT

The authors would like to express thanks to **Prof. Koneru S R**, Retired Professor, Department of Mathematics, IIT Bombay, for his support throughout this research work.

NOMENCLATURE

a,c	Constants	u_w	Velocity of the stretching sheet
Bi	Biot number	u,v	Cartesian coordinates (x axis is aligned along the stretching surface and y axis is the normal to it)
C_f	Skin friction coefficient	α	Thermal diffusivity
C_w	Nanoparticles volume fraction at the stretching sheet	β	Dimensionless nanoparticles volume fraction

C_∞	Ambient nanoparticles volume	η	Similarity variable
D_B	Brownian diffusion coefficient	θ	Dimensionless temperature
D_T	Thermophoresis diffusion coefficient	χ	Chemical reaction parameter
Ec	Eckert number	ν	Kinematic viscosity of the fluid
$f(\eta)$	Dimensionless stream function	ρ_f	Fluid density
κ	Thermal conductivity	ρ_p	Nanoparticle mass density
Nb	Brownian motion parameter	σ	Electrical conductivity of the fluid
Nt	Thermophoresis parameter	τ	Parameter defined by ratio between the effective heat capacity of the nanoparticle material and heat capacity of the fluid. $\tau = (\rho c)_p/(\rho c)_f$.
Nu	Nusselt number	k^*	mean absorption
Nur	Reduced Nusselt number	T_w	Temperature at the stretching sheet
Pr	Prandtl number	T_∞	Ambient temperature
p	Fluid pressure	C_∞	Ambient nanoparticle volume fraction
μ	dynamic viscosity	C_w	Nanoparticle volume fraction at the stretching sheet
σ^*	Stefan-Boltzmann constant	ψ	Stream function
$(\rho C)_f$	Heat capacity of the fluid	∞	Condition at the free stream
$(\rho C)_p$	Effective heat capacity of the nanoparticle material	w	Condition of the surface
q_m	Wall mass flux	Ra	radiation parameter
q_w	Wall heat flux	Pr	Prandtl number
Re_x	Local Reynolds number	Le	Lewis number
Shr	Reduced Sherwood number	M	magnetic parameter
Sh_x	Local Sherwood number	Bi	Biot number
T	Fluid temperature	τ_w	shear stress

REFERENCES

1. SUS Choi. **1995**. "Enhancing thermal conductivity of fluids with nanoparticles". *ASME-Publications-Fed*, **231**: 99-106.
2. Jastman, J.A., Phillpot, S.R., Choi, S.U.S. and Keblinski, P. **2004**. "Thermal transport in nanofluids". *Annu. Rev. Mater. Res*., **34**: 219-246.
3. Buongiorno, J. **2006.** "Convective transport in nanofluids". *J HEAT TRANSF*, **128**(3): 240-250.
4. Kuznetsov, A.V. and Nield. **2010.** Natural convective boundary-layer flow of a nanofluid past a vertical plate". *INT J THERM SCI*, **49**(2): 243-247.
5. Kuznetsov, A.V. and Nield, D.A. **2014**. "Natural convective boundary-layer flow of a nanofluid past a vertical plate": A revised model. *INT J THERM SCI*, **77**: 126-129.
6. Krishna, P.M., Sandeep, N. and Sugunamma, V. **2015**. "Effects of radiation and chemical reaction on MHD convective flow over a permeable stretching surface with suction and heat generation". *Web Journey Science and Technology*, **12**: 831-847.

7. Abbas, Z., Naveed, M. and Sajid, M. **2016**. "Hydromagnetic slip flow of nanofluid over a curved stretching surface with heat generation and thermal radiation". *Journal of Molecular Liquids*, **215**: 756-762.

8. Haq, R.U., Nadeem, S., Khan, Z.H. and Akbar, N.S. **2015**. "Thermal radiation and slip effects on MHD stagnation point flow of nanofluid over a stretching sheet". *Physics E*, **65**: 27-23.

9. Sheikholeslami, M., Ganji, D.D., Javed, M.Y. and Ellahi, R. **2015**. "Effect of thermal radiation on magnetohydrodynamics nanofluid flow and heat transfer by means of two-phase model". *Journal of Magnetism and Magnetic Materials*, **374**: 36-43.

10. Magyari, E. and Chamkha, A.J. **2010**. "Combined effect of heat generation or absorption and first-order chemical reaction on micropolar fluid flows over a uniformly stretched permeable surface: The full analytical solution". *International Journal of Thermal Sciences*, **49(9)**: 1821-1828.

11. Devi, S.P.A. and Kandasamy, R. **2001**. "Thermal stratification effects on laminar boundary-layer flow over a wedge with suction or injection". *Mechanics Research Communications*, **28(3)**: 349-354.

12. Chamkha and, A.J. Rashad, A.M. **2014**. "Unsteady heat and mass transfer by MHD mixed convection flow from a rotating vertical cone with chemical reaction and soret and dufour effects". *The Canadian Journal of Chemical Engineering*, **92**(4): 758-767, 2014.

13. Fox, R.W. and Mcdonald, A.T. and Pritchard, P.J. **2004**. "Introduction to fluid mechanics". sixth Edition, John Wiley and Sons, Inc. 2004.

14. Sreenivasulu, B., Kirti, N.S., Krishna, G.V., Sree, B.R. and Ramesh, K.V. **2017**. "A numerical study on enhanced heat transfer in a lid driven cavity with and without fins". International conference of Electronics, Communication and Aerospace Technology, **2**: 611-616.

15. Bar-Meir, G. **2013**. "*Basics of fluid mechanics*". Potto Project.

16. Gbadeyan, J.A. Olanrewaju, M.A. and Olanrewaju, P.O. **2011**. "Boundary Layer Flow of a nanofluid Past a Stretching Sheet with a Convective Boundary Condition in the Presence of Magnetic Field and Thermal Radiation". *Australian Journal of Basic and Applied Sciences*, **5(9)**: 1323-1334.